

Communication

Highly Reliable Temperature Sensor Based on p-GaN/AlGaN/GaN Hybrid Anode Diode with Wide Operation Temperature from 73 K to 573 K

An Yang^{1,2,3}, Xing Wei^{1,3}, Wenchao Shen³, Yu Hu^{2,3}, Tiwei Chen^{1,3}, Heng Wang³, Jiaan Zhou³, Runxian Xing³, Xiaodong Zhang^{1,3,4}, Guohao Yu^{1,3}, Yaming Fan^{3,4}, Yong Cai^{1,3}, Zhongming Zeng^{1,3,4} and Baoshun Zhang^{1,3,*}

¹ School of Nano-Tech and Nano-Bionics, University of Science and Technology of China, Hefei 230026, China

² Nano Science and Nano Technology Institute, University of Science and Technology of China, Suzhou 215123, China

³ Nanofabrication Facility, Suzhou Institute of Nano-Tech and Nano-Bionics, Chinese Academy of Sciences, Suzhou 215123, China

⁴ Nanchang Key Laboratory of Advanced Packaging and the Division of Nano-Devices and Technologies, Jiangxi Institute of Nanotechnology, Nanchang 330200, China

* Correspondence: bszhang2006@sinano.ac.cn

Abstract: A high-performance temperature sensor based on a p-GaN/AlGaN/GaN hybrid anode diode (HPT-HAD) fabricated by hydrogen plasma treatment is demonstrated. The sensor exhibits accurate and stable temperature responses from 73 to 573 K. The forward anode voltage is linearly proportional to the temperature over the measured temperature range at a fixed current. At a forward current density of 10^{-7} mA/mm, the device achieves a maximum sensitivity of 1.93 mV/K. The long-time anode current stress measurement reveals that the HPT-HAD shows almost no degradation even at 573 K for 1 h at a current of 100 μ A, and the anode voltage shifts only 120 mV at 573 K for 1000 s at 1 nA. This work shows that the HPT-HAD temperature sensor can be reliably operated over a wide temperature range from cryogenic to high temperatures, so can be used in a variety of extreme environments.

Keywords: p-GaN/AlGaN/GaN; temperature sensor; semiconductor materials



Citation: Yang, A.; Wei, X.; Shen, W.; Hu, Y.; Chen, T.; Wang, H.; Zhou, J.; Xing, R.; Zhang, X.; Yu, G.; et al.

Highly Reliable Temperature Sensor Based on p-GaN/AlGaN/GaN Hybrid Anode Diode with Wide Operation Temperature from 73 K to 573 K. *Crystals* **2023**, *13*, 620. <https://doi.org/10.3390/cryst13040620>

Academic Editor: Francisco M. Morales

Received: 1 March 2023

Revised: 26 March 2023

Accepted: 29 March 2023

Published: 4 April 2023



Copyright: © 2023 by the authors. Licensee MDPI, Basel, Switzerland. This article is an open access article distributed under the terms and conditions of the Creative Commons Attribution (CC BY) license (<https://creativecommons.org/licenses/by/4.0/>).

1. Introduction

Temperature is one of the most essential and fundamental physical quantities. Both direct and indirect methods can be utilized to obtain temperature parameters [1]. Commonly used direct temperature-sensing techniques include optical methods, physical contact methods, and electrical methods [2]. The utilization of a p-GaN high electron mobility transistor (HEMT) in power integrated circuits is already well-established in the commercial industry; however, detecting their operational status and promptly notifying of malfunctions in real-time has been an ongoing challenge [3]. An integratable temperature-sensing module for real-time temperature monitoring can help to detect and predict the failure of critical components in a timely manner [4,5]. GaN is a promising semiconductor material for extreme-environment-sensing applications due to its wide bandgap (3.4 eV) and performance stability [6,7]. GaN diodes have been previously demonstrated as viable temperature sensors [8–15]; however, there are very few reports on the design and fabrication of temperature sensors on the AlGaN/GaN platform [14,16]. In order to achieve real-time monitoring of the operating temperature of power integrated circuits, we require a compact device that can be easily integrated into a p-GaN HEMT. Our designed lateral hybrid anode diode (HAD) is substrate consistent with a conventional p-GaN HEMT for power integrated circuits and is manufactured with fully compatible processes. In our previous work, HAD temperature sensors on the commercial p-GaN HEMT platform were

reported with a temperature range from room temperature to 473 K [17]. However, certain extreme applications necessitate the operation of these devices at cryogenic temperatures as low as that of liquid nitrogen (~ 77 K), such as aerospace, quantum computing, and extreme-environment exploration [18–20]. Therefore, temperature sensors that can reliably measure a wide temperature range from cryogenic to high temperature are highly beneficial for these applications.

In this paper, a high-performance temperature sensor based on a p-GaN/AlGa_xN/GaN hybrid anode diode (HPT-HAD) fabricated by self-aligned etching-free hydrogen plasma treatment is demonstrated and comprehensively characterized from 73 to 573 K. It should be noted that the temperature range is limited by the Janis Cryogenic Probe System, not by the device itself. The forward anode voltage below the zero-temperature coefficient (ZTC) point is linearly proportional to the temperature over the measured temperature range with a maximum sensitivity of 1.93 mV/K at a current density of 10^{-7} mA/mm. The HPT-HAD showed good long-time-stress reliability even at 573 K for 1 h.

2. Materials and Methods

2.1. Epitaxial Structure

The heterostructure epitaxy materials utilized in this study were grown on a 2-inch silicon (111) substrate using metal organic chemical vapor deposition (MOCVD).

The epitaxial structure on which the HPT-HAD device was based is illustrated in Figure 1a, as depicted. We first grew a layer of amorphous GaN nucleation sites on the Si substrate via MOCVD at a low temperature of 500 °C. Next, we performed a rapid annealing step at 1100 °C for five minutes, which facilitated the recrystallization of GaN along the crystalline phase of the Si substrate. We then grew a buffer layer of Al_xGa_{1-x}N at a higher temperature of 1050 °C, which was doped with carbon to minimize background carrier concentration and withstand stress. To increase device mobility and reduce scattering of 2DEG by the buffer layer, we grew a layer of high-quality intrinsic GaN crystals as a transport channel for the electrons. Additionally, we inserted a thin layer of AlN between the potential and channel layers to reduce the effect of alloy scattering from the AlGa_xN ternary material and improve electron mobility. To balance the concentration of 2DEG and reduce stress in the barrier layer, we grew an 18 nm thick Al_{0.2}Ga_{0.8}N layer with an Al fraction of 0.2. Finally, we grew a 70 nm thick p-GaN cap layer doped with Mg at approximately 4×10^{19} cm⁻³. Figure 2b demonstrates that p-GaN grown using this method possesses excellent surface roughness with an RMS value of 0.26 nm.

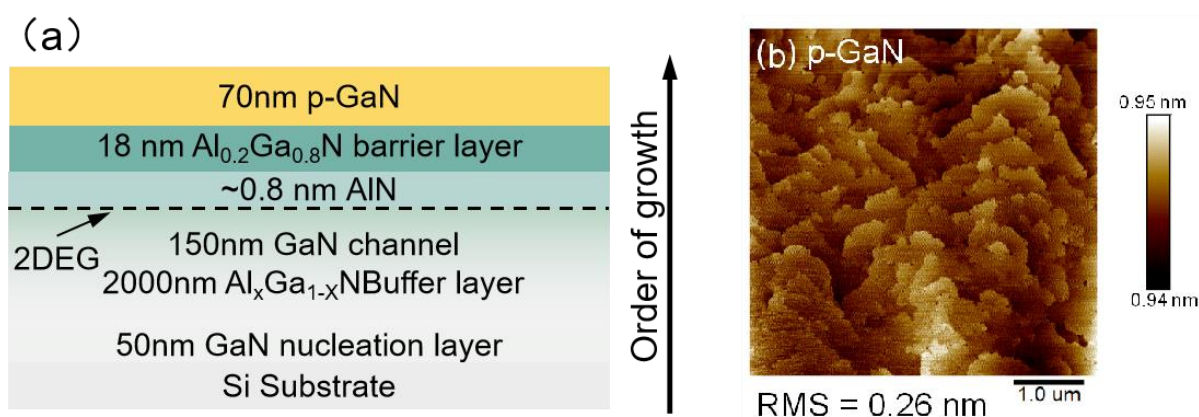


Figure 1. (a) Cross-sectional schematic of epi-structure; (b) AFM image of p-GaN MOCVD growth.

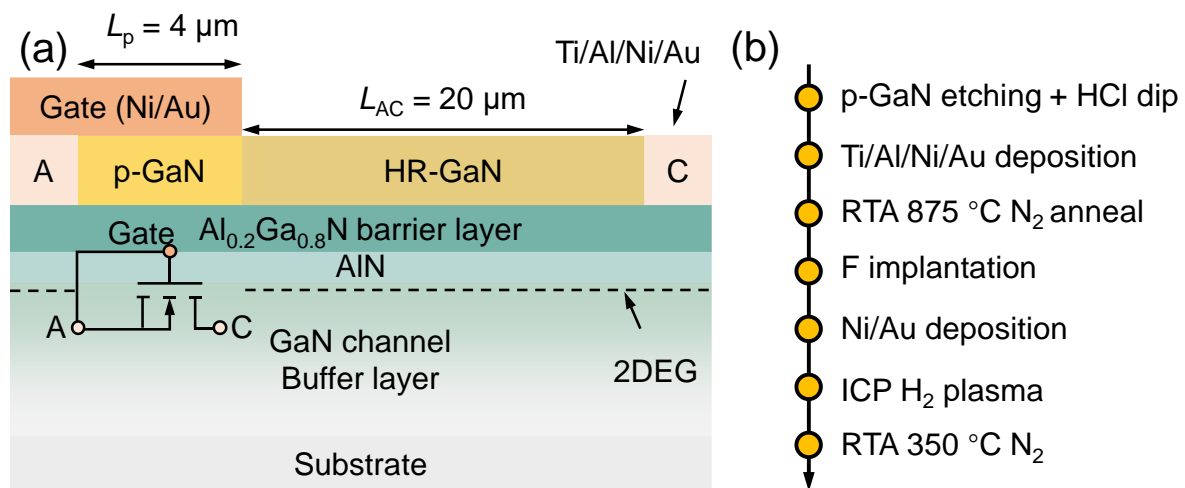


Figure 2. (a) Cross-sectional schematic of the HPT-HAD; (b) fabrication process for the HPT-HAD.

2.2. Device Structure and Manufacturing Methods

Figure 2a illustrates the structure of the temperature sensor based on HPT-HAD. The p-GaN/AlGa_{0.2}N/AlN/GaN (70 nm/18 nm/~0.8 nm/~2 μm) epi-structure was grown on a 2-inch silicon substrate by metal-organic chemical vapor deposition, and the Mg-doping concentration of a p-GaN cap layer was about $4 \times 10^{19} \text{ cm}^{-3}$. The hybrid anode consists of the ohmic anode metal in contact with the two-dimensional electron gas (2DEG) and the p-GaN, and the gate metal connecting the p-GaN to the anode metal. Thus, the HPT-HAD is equivalent to a gate-to-source connected transistor.

The HPT-HAD was fabricated using traditional optical photolithography as shown in Figure 2b. It began with removing the p-GaN layer on the anode- and cathode-contact area by dry etching. Before the Ti/Al/Ni/Au metal stack deposition by electron beam evaporation, the sample was briefly dipped in diluted hydrochloric acid (HCl) to remove native surface oxides. The ohmic anode and cathode were formed after rapid thermal annealing (RTA) at 850 °C in N₂ ambient. The device isolation was realized by fluorine implantation. The Ni/Au gate was evaporated on the p-GaN and ohmic anode. To form high-resistivity GaN (HR-GaN), the sample was load into the Oxford Plasmalab System 100 ICP 180 for H₂ plasma treatments where the metal electrodes serve as hard masks, followed by thermal annealing by RTA at 623 K in N₂ ambient. The procedure of passivating H plasma is proficient in assuaging etching while transforming the processed GaN into a protective layer of high resistance. This modality engenders notable abatements in the deleterious impacts of etching, superficial state defects, and lattice fit defects, thereby amplifying the stability of devices and ameliorating the reverse leakage current. The treatment conditions were the same as the previous works [17,21]. Concomitantly, the Ni/Au metallic gate functions as a robust mask, preserving the p-type doping characteristics of the GaN beneath it from the H plasma processing. The minute segment of p-GaN that endures is able to exhaust the 2DEG below, adroitly regulating device turn-off. The reduced defects also mitigate the hot carrier effect at elevated temperatures, endowing our devices with improved thermal stability. The HPT-HADs had an p-GaN length (L_p) of 4 μm, an anode-to-cathode length (L_{AC}) of 20 μm, and a width of p-GaN gate (W_G) of 100 μm. No surface passivation was employed in the devices. The current-voltage (I - V) characteristics of the HPT-HAD temperature sensor were measured using Keysight B1500A semiconductor analyzer system and Janis Cryogenic Probe System from 73 to 573 K.

To validate the superior surface quality preservation achieved through H plasma as opposed to traditional ICP etching, we conducted separate H plasma and ICP etching procedures on a single p-GaN substrate. The stark contrast observed in Figure 3a,b provides compelling evidence that the H plasma treatment inflicts far less damage on the material surface compared to ICP etching.

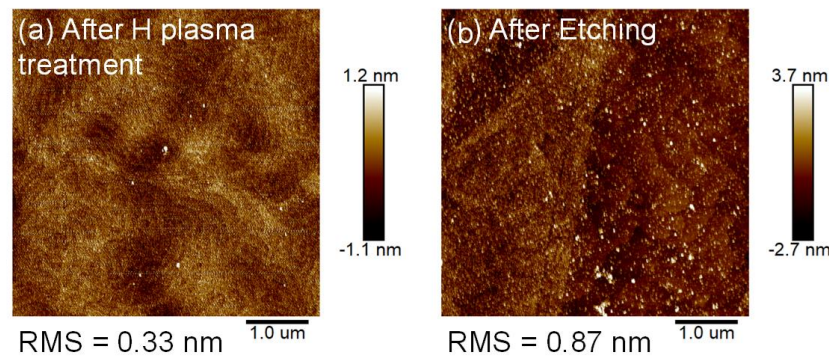


Figure 3. AFM image of (a) after H plasma treatment, and (b) after ICP Etching.

3. Results

3.1. Performance and Principle

Figure 4a shows the temperature-dependent forward $I-V$ characteristics of the HPT-HAD temperature sensor in a semi-log scale from 73 to 573 K. The HPT-HAD exhibited good rectifying behaviors at all measured temperatures. The current density of the device decreased as the temperature increased, which is due to the enhanced phonon scattering and thus reduced carrier mobility at high temperatures [22]. The OFF-state current density of the device was as low as 10 pA/mm, and the I_{ON}/I_{OFF} ratio was $10^9 \sim 10^{11}$, which can be ascribed to the low surface damage by the etching-free plasma treatment technology. The HPT-HAD sensor showed a zero-temperature coefficient (ZTC) bias point of 1.6 V at which the device exhibited minimum temperature sensitivity, which is similar to reported devices [13,16].

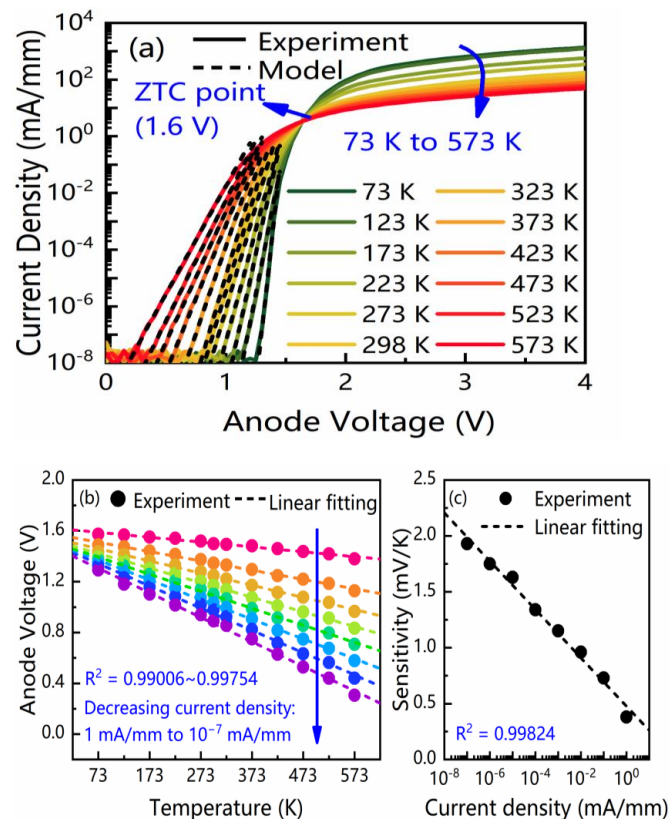


Figure 4. (a) Forward $I-V$ characteristics of the HPT-HAD temperature sensor in semi-log scale at different temperatures (73 to 573 K). (b) The forward anode voltage against with different fixed current density levels at all temperatures. (c) The sensitivity versus current density in semi-log scale.

Figure 4b presents the forward anode voltage (V_A) across the HPT-HAD against temperature (T) at different fixed low current density (I_A) levels. A highly linear relationship between the V_A and T with a negative temperature coefficient from 73 to 573 K was observed, indicating that the HPT-HAD sensors can operate in a wide temperature range from cryogenic to high temperatures. This test is a step-by-step progression from the low temperature to the high temperature. The sensitivity (S) of the devices was defined as the temperature coefficient extracted from the linear fitting curves. Figure 4c depicts the device sensitivity at different current density levels. The device sensitivities at eight I_A of 1, 10^{-1} , 10^{-2} , 10^{-3} , 10^{-4} , 10^{-5} , 10^{-6} , and 10^{-7} mA/mm were extracted as 0.38, 0.73, 0.96, 1.15, 1.34, 1.63, 1.75, and 1.93 mV/K, respectively. The relationship between the device sensitivity and the current density level can be expressed as follows: $S \propto \ln(I_A)$.

Based on the thermionic emission theory, the Schottky diode's I - V relationship can be expressed as [23]

$$I = AA^*T^2 \exp\left(-\frac{q\phi_B}{kT}\right) \left[\exp\left(\frac{qV}{kT}\right) - 1 \right] \quad (1)$$

$$I_S = AA^*T^2 \exp\left(-\frac{q\phi_B}{kT}\right) \quad (2)$$

where A represents the Schottky junction's area, A^* is the effective Richardson constant, and the A^* value for GaN is 26.3 A/(cm²·K²) at 300 K. For AlGaIn materials with Al compositions of 20%, the corresponding A value is 32.6 A/(cm²·K²). Here, ϕ_B is the height of the Schottky barrier at zero bias, and I_S represents the reverse saturation current.

When considering non-ideal effects such as image force, tunneling, recombination current of electron-hole pairs, hole injection effect, and series resistance, the IV equation can be expressed as [24,25]

$$I = AA^*T^2 \exp\left(-\frac{q\phi_B}{kT}\right) \left[\exp\left(\frac{qV - IR_S}{nkT}\right) - 1 \right] \quad (3)$$

In Equation (3), n represents the ideality factor, and R_S is the equivalent series resistance of the current path. When V is greater than 3 kT/q, the equivalent series resistance R_S is relatively small and can be simplified to

$$I = AA^*T^2 \exp\left(-\frac{q\phi_B}{kT}\right) \exp\left(\frac{qV}{nkT}\right) \quad (4)$$

By taking the logarithm of both sides of Equations (3) and (4), we can obtain

$$\lg I = \frac{q\lg e}{kT} \cdot \frac{1}{n} \cdot V + \lg AA^*T^2 + \lg e \cdot \frac{-q\phi_B}{kT} \quad (5)$$

The barrier height and ideality factor can be extracted from the slope and intercept of the $\lg I$ - V curve on a semi-logarithmic coordinate system, yielding:

$$\phi_B = \frac{kT}{q\lg e} \cdot \lg \frac{AA^*T^2}{\text{intercept}} \quad (6)$$

$$n = \frac{q\lg e}{kT} \cdot \frac{1}{\text{slope}} \quad (7)$$

Based on temperature-dependent testing results and the aforementioned calculation formula, we extracted the Schottky barrier and ideality factor of the device from 273 K to 523 K. As shown in Figure 5, the Schottky barrier of the device continues to rise while the ideality factor gradually approaches 1 as the temperature increases. This trend of the Schottky diode barrier and ideality factor variation with temperature is consistent with that reported in other articles [26].

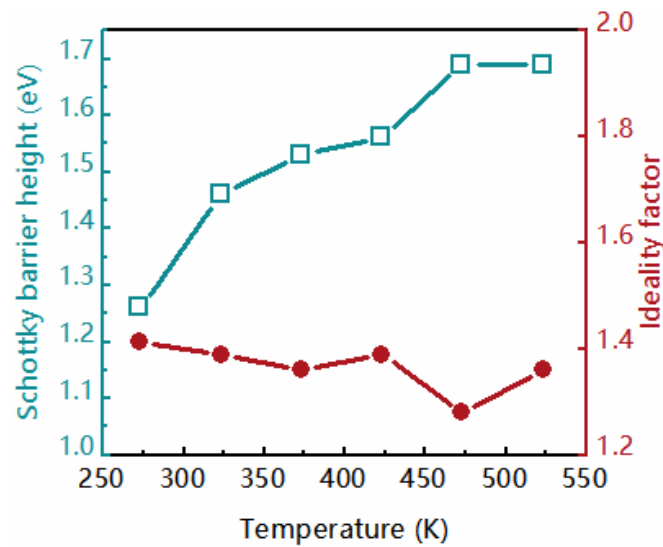


Figure 5. The calculation results of the Schottky barrier and ideality factor of the device.

3.2. Reliability and Comparison

To evaluate the long-time reliability of the HPT-HAD temperature sensor, the device was measured under the anode current stress for a long time at high temperatures [27]. Figure 6 shows the changes in V_A (ΔV_A) at different temperatures for 1 h with the anode current density of 1 mA/mm. This suggests that the V_A drifted negatively and more significantly with increasing temperature under the anode current stress and the highest ΔV_A were only -1.60 , -1.71 , -2.87 , and -2.89 mV at 298, 373, 473, and 573 K, respectively.

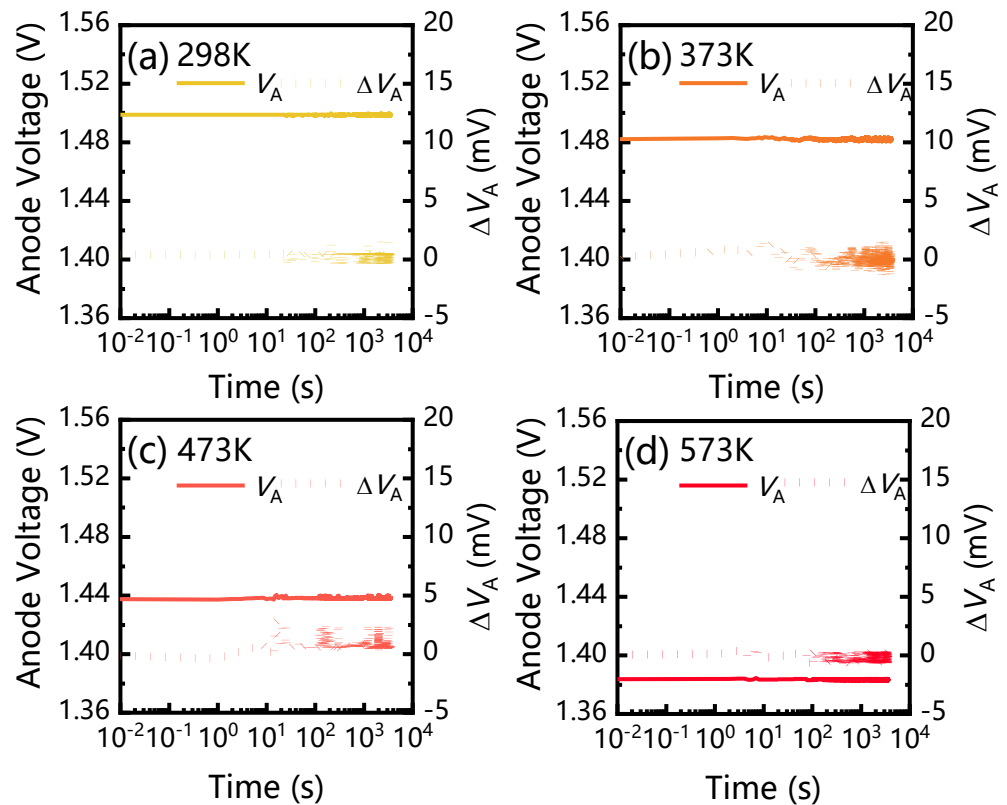


Figure 6. Shift in Anode voltage during forward current densities of 1 mA/mm at (a) 298 K, (b) 373 K, (c) 473 K, and (d) 573 K.

Figure 7 shows the ΔV_A at different anode current stresses for 1000 s at 573, 298 and 73 K. At 573 K, the V_A showed almost no change at high current density ($\geq 10 \mu\text{A}/\text{mm}$) and shifted negatively by about 120 mV at low current density ($< 10 \mu\text{A}/\text{mm}$). At 73 K, the device exhibited excellent long-term stability, with almost no performance drift observed. This may be because defects are frozen at 73 K, and the performance drift caused by carrier thermal effects cannot accumulate. At room temperature, this device also demonstrated impressive stability, which may be attributed to the reduction of defects. These results indicate the high reliability of the HPT-HAD temperature sensors.

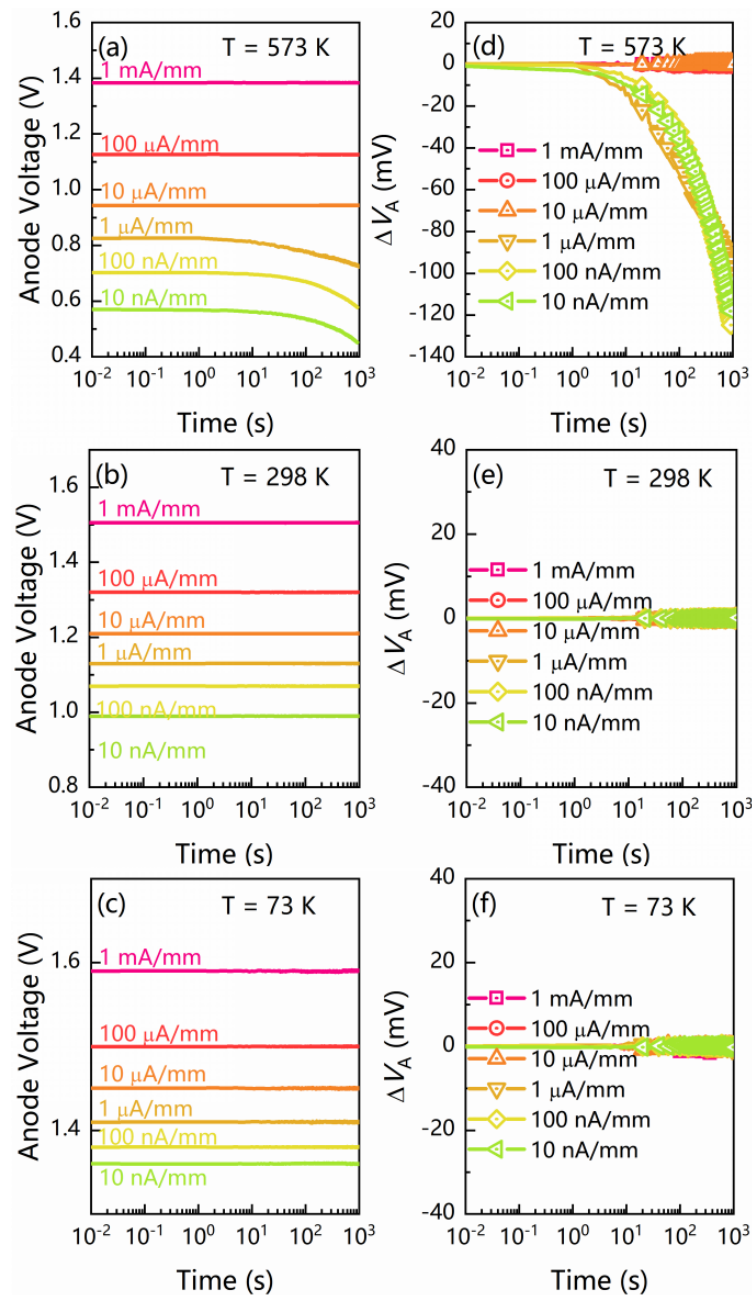


Figure 7. Anode voltage over time measured during different forward current densities at (a) 573 K, (b) 298 K, (c) 73 K and shift in anode voltage measured during different forward current densities at (d) 573 K, (e) 298 K, (f) 73 K.

As shown in Figure 8, the performance of our device was benchmarked against some state-of-the-art temperature sensors based on AlGaIn/GaN diodes [8,10–17]. Our HPT-HAD temperature sensor demonstrated sensitivity of 1.93 mV/K and a broad operating

temperature range from 73 to 573 K. Moreover, the device showed remarkable stability at 73, 298, and 573 K. This desirable performance is mainly attributed to the H plasma treatment employed during the device fabrication process, which mitigates etching-induced damage and minimizes defects. Moreover, the H-treated p-GaN also serves to passivate and protect the device to some extent. Our previous work has confirmed the effectiveness of this approach [28].

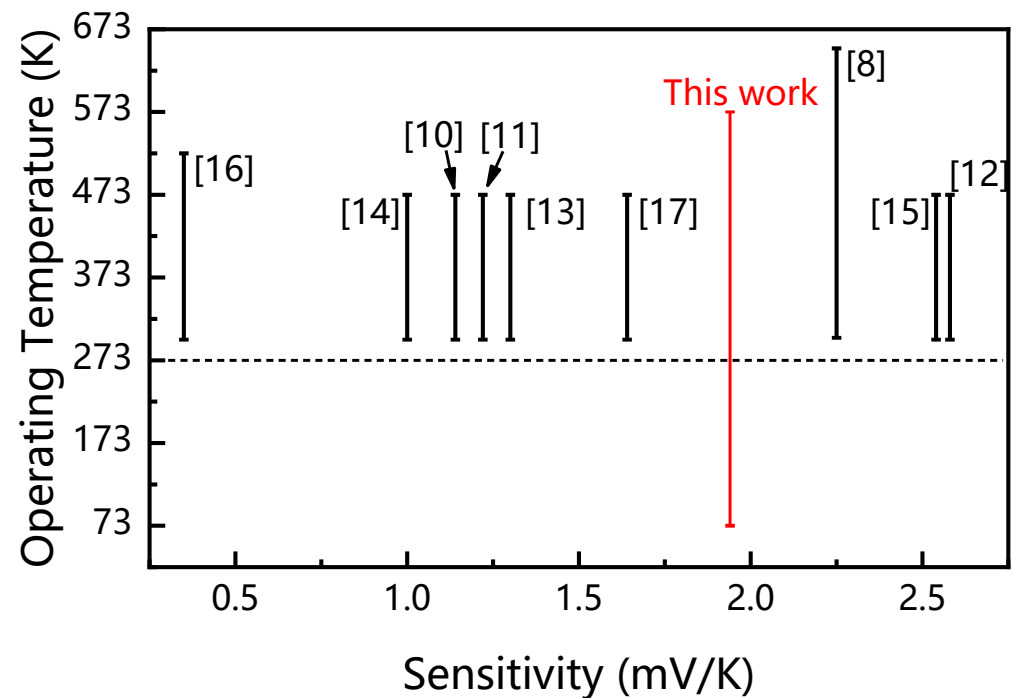


Figure 8. Operating temperature vs. sensitivity for HPT-HAD temperature sensor compared with some reported state-of-the-art AlGaIn/GaN diode temperature sensors.

4. Conclusions

In summary, we demonstrated a temperature sensor based on HPT-HAD that can operate from 73 to 573 K. The temperature sensor maintained a good linear relationship between forward anode voltage and temperature with a sensitivity of 1.93 mV/K. The experimental results were supported by an analytical model. Almost no forward anode voltage degradation during a long-time current stress test even at 573 K showed the high reliability of the HPT-HAD temperature sensors. These results indicate that the HPT-HAD is a promising candidate for temperature sensors in extreme environments.

Author Contributions: Conceptualization, A.Y. and B.Z.; methodology, A.Y.; software, X.W.; validation, W.S., Y.H. and T.C.; formal analysis, H.W.; investigation, J.Z.; resources, R.X.; data curation, X.Z.; writing—original draft preparation, A.Y.; writing—review and editing, G.Y.; visualization, Y.F.; supervision, Y.C.; project administration, Z.Z. All authors have read and agreed to the published version of the manuscript.

Funding: This work was supported in part by the National Key Research and Development Program of China (Grant No. 2021YFB3600202), the Fundamental Research Funds for the Central Universities (Grant No. WK5290000003), National Natural Science Foundation of China (Grant No. U1830112), Natural Science Foundation Key Project of Jiangxi Province, China (Grant No. 20202ACBL202001), Key Laboratory Construction Project of Nanchang (Grant No. 2020-NCZDSY-008), Jiangxi Province Double Thousand Plan (Grant No. S2019CQKJ2638). The authors would like to thank the Nano Fabrication Facility, the Platform for Characterization and Testing, Vacuum Interconnected Nanotech Workstation (NANO-X), and Suzhou Institute of Nano-Tech and Nano-Bionics, Chinese Academy of Sciences.

Conflicts of Interest: The authors declare no conflict of interest.

References

1. Trung, T.Q.; Lee, N.-E. Flexible and Stretchable Physical Sensor Integrated Platforms for Wearable Human-Activity Monitoring and Personal Healthcare. *Adv. Mater.* **2016**, *28*, 4338–4372. [[CrossRef](#)]
2. Blackburn, D. Temperature Measurements of Semiconductor Devices—A Review. In Proceedings of the 20th Annual IEEE Semiconductor Thermal Measurement and Management Symposium, San Jose, CA, USA, 9–11 March 2004; p. 70. [[CrossRef](#)]
3. Udrea, F.; Santra, S.; Gardner, J.W. CMOS temperature sensors—Concepts, state-of-the-art and prospects. In Proceedings of the 31st International Semiconductor Conference, Sinaia, Romania, 13–15 October 2008; p. 31. [[CrossRef](#)]
4. Kalker, S.; Ruppert, L.A.; van der Broeck, C.H.; Kuprat, J.; Andresen, M.; Polom, T.A.; Liserre, M.; De Doncker, R.W. Reviewing Thermal-Monitoring Techniques for Smart Power Modules. *IEEE J. Emerg. Sel. Top. Power Electron.* **2021**, *10*, 1326–1341. [[CrossRef](#)]
5. Yang, F.; Pu, S.; Xu, C.; Akin, B. Turn-on Delay Based Real-Time Junction Temperature Measurement for SiC MOSFETs With Aging Compensation. *IEEE Trans. Power Electron.* **2020**, *36*, 1280–1294. [[CrossRef](#)]
6. Chu, R. GaN power switches on the rise: Demonstrated benefits and unrealized potentials. *Appl. Phys. Lett.* **2020**, *116*, 090502. [[CrossRef](#)]
7. Chen, K.J.; Haberlen, O.; Lidow, A.; Tsai, C.L.; Ueda, T.; Uemoto, Y.; Wu, Y. GaN-on-Si Power Technology: Devices and Applications. *IEEE Trans. Electron Devices* **2017**, *64*, 779–795. [[CrossRef](#)]
8. Madhusoodhanan, S.; Sandoval, S.; Zhao, Y.; Ware, M.E.; Chen, Z. A Highly Linear Temperature Sensor Using GaN-on-SiC Heterojunction Diode for High Power Applications. *IEEE Electron Device Lett.* **2017**, *38*, 1105–1108. [[CrossRef](#)]
9. Li, L.; Chen, J.; Gu, X.; Li, X.; Pu, T.; Ao, J.-P. Temperature sensor using thermally stable TiN anode GaN Schottky barrier diode for high power device application. *Superlattices Microstruct.* **2018**, *123*, 274–279. [[CrossRef](#)]
10. Li, X.; Pu, T.; Li, L.; Ao, J.-P. Enhanced Sensitivity of GaN-Based Temperature Sensor by Using the Series Schottky Barrier Diode Structure. *IEEE Electron Device Lett.* **2020**, *41*, 601–604. [[CrossRef](#)]
11. Li, X.; Pu, T.; Li, X.; Li, L.; Ao, J.-P. Correlation Between Anode Area and Sensitivity for the TiN/GaN Schottky Barrier Diode Temperature Sensor. *IEEE Trans. Electron Devices* **2020**, *67*, 1171–1175. [[CrossRef](#)]
12. Li, X.; Pu, T.; Zhang, T.; Li, X.; Li, L.; Ao, J.-P. p-NiO/n-GaN Heterostructure Diode for Temperature Sensor Application. *IEEE Sens. J.* **2019**, *20*, 62–66. [[CrossRef](#)]
13. Li, L.; Li, X.; Pu, T.; Cheng, S.; Li, H.; Ao, J.-P. Vertical GaN-Based Temperature Sensor by Using TiN Anode Schottky Barrier Diode. *IEEE Sens. J.* **2020**, *21*, 1273–1278. [[CrossRef](#)]
14. Pu, T.; Li, X.; Wu, J.; Yang, J.; Lu, Y.; Liu, X.; Ao, J.-P. Recessed Anode AlGaIn/GaN Schottky Barrier Diode for Temperature Sensor Application. *IEEE Trans. Electron Devices* **2021**, *68*, 5162–5166. [[CrossRef](#)]
15. Li, L.; Pu, T.; Li, X.; Ao, J.-P. Effect of Anode Material on the Sensitivity of GaN Schottky Barrier Diode Temperature Sensor. *IEEE Sens. J.* **2021**, *22*, 1933–1938. [[CrossRef](#)]
16. Kwan, A.M.H.; Guan, Y.; Liu, X.; Chen, K.J. A Highly Linear Integrated Temperature Sensor on a GaN Smart Power IC Platform. *IEEE Trans. Electron Devices* **2014**, *61*, 2970–2976. [[CrossRef](#)]
17. Wei, X.; Zhang, X.; Zhou, X.; Ma, Y.; Tang, W.; Chen, T.; Liu, W.; Tang, W.; Yu, G.; Fan, Y.; et al. Dual Current and Voltage Sensitivity Temperature Sensor Based on Lateral p-GaN/AlGaIn/GaN Hybrid Anode Diode. *IEEE Sens. J.* **2021**, *21*, 22459–22463. [[CrossRef](#)]
18. Rajashekara, K.; Akin, B. A review of cryogenic power electronics—Status and applications. In Proceedings of the IEEE International Electric Machines and Drives Conference (IEMDC), Chicago, IL, USA, 12–15 May 2013; pp. 899–904. [[CrossRef](#)]
19. Gui, H.; Chen, R.; Niu, J.; Zhang, Z.; Tolbert, L.M.; Wang, F.F.; Blalock, B.J.; Costinett, D.; Choi, B.B. Review of Power Electronics Components at Cryogenic Temperatures. *IEEE Trans. Power Electron.* **2019**, *35*, 5144–5156. [[CrossRef](#)]
20. Nela, L.; Perera, N.; Erine, C.; Matioli, E. Performance of GaN Power Devices for Cryogenic Applications Down to 4.2 K. *IEEE Trans. Power Electron.* **2020**, *36*, 7412–7416. [[CrossRef](#)]
21. Wei, X.; Shen, W.; Zhou, X.; Tang, W.; Ma, Y.; Chen, T.; Wang, D.; Fu, H.; Zhang, X.; Lin, W.; et al. 2.69 kV/2.11 mΩ·cm² and Low Leakage p-GaN Stripe Array Gated Hybrid Anode Diodes with Low Turn-on Voltage. *IEEE Electron Device Lett.* **2022**, *44*, 13–16. [[CrossRef](#)]
22. Fu, H.; Fu, K.; Liu, H.; Alugubelli, S.R.; Huang, X.; Chen, H.; Montes, J.; Yang, T.-H.; Yang, C.; Zhou, J.; et al. Implantation- and etching-free high voltage vertical GaN p-n diodes terminated by plasma-hydrogenated p-GaN: Revealing the role of thermal annealing. *Appl. Phys. Express* **2019**, *12*, 051015. [[CrossRef](#)]
23. Mansoor, M.; Haneef, I.; Akhtar, S.; De Luca, A.; Udrea, F. Silicon diode temperature sensors—A review of applications. *Sens. Actuators A Phys.* **2015**, *232*, 63–74. [[CrossRef](#)]
24. Zhang, N.; Lin, C.-M.; Senesky, D.G.; Pisano, A.P. Temperature sensor based on 4H-silicon carbide pn diode operational from 20 °C to 600 °C. *Appl. Phys. Lett.* **2014**, *104*, 073504. [[CrossRef](#)]
25. Schmitz, A.C.; Ping, A.T.; Khan, M.A.; Chen, Q.; Yang, J.W.; Adesida, I. Schottky barrier properties of various metals on n-type GaN. *Semicond. Sci. Technol.* **1996**, *11*, 1464–1467. [[CrossRef](#)]
26. Bian, Z.; Su, K.; Zhang, J.; Zhao, S.; Zhou, H.; Zhang, W.; Zhang, Y.; Zhang, T.; Chen, J.; Dang, K.; et al. Gamma irradiation impact on GaN quasi-vertical Schottky barrier diodes. *J. Phys. D Appl. Phys.* **2019**, *53*, 045103. [[CrossRef](#)]

27. De Luca, A.; Pathirana, V.; Ali, S.Z.; Udrea, F. Silicon on insulator thermodiode with extremely wide working temperature range. In Proceedings of the 2013 Transducers & Eurosensors XXVII: 17th International Conference on Solid-State Sensors, Actuators and Microsystems (Transducers & Eurosensors XXVII), Barcelona, Spain, 16–20 June 2013; p. 1911. [[CrossRef](#)]
28. Wei, X.; Zhang, X.; Tang, W.; Liu, W.; Zhou, X.; Tang, W.; Ma, Y.; Chen, T.; Huang, X.; Qian, H.; et al. 2.0 kV/2.1 mΩ·cm² Lateral p-GaN/AlGaN/GaN Hybrid Anode Diodes with Hydrogen Plasma Treatment. *IEEE Electron Device Lett.* **2022**, *43*, 693–696. [[CrossRef](#)]

Disclaimer/Publisher’s Note: The statements, opinions and data contained in all publications are solely those of the individual author(s) and contributor(s) and not of MDPI and/or the editor(s). MDPI and/or the editor(s) disclaim responsibility for any injury to people or property resulting from any ideas, methods, instructions or products referred to in the content.